

# A hybrid model to calculate the magnetization of nanostructured permanent magnetic materials

G.P. Zhao <sup>a,\*</sup>, H.S. Lim <sup>b</sup>, Y.P. Feng <sup>b</sup>, C.K. Ong <sup>b</sup>

<sup>a</sup> Department of Material Science, National University of Singapore, Singapore 119260, Singapore

<sup>b</sup> Center for Superconductivity and Magnetic Materials, Department of Physics, National University of Singapore, Singapore 119260, Singapore

Received 12 December 2003; accepted 20 February 2004

## Abstract

We present our simulated initial magnetization curves for nanostructured permanent magnets based on a simple hybrid model. The model assumes that the reversible change in the magnetization curves obeys the Stoner–Wohlfarth (SW) model while the irreversible part can be attributed to the motion of the transition region (TR), which is a domain-wall-like magnetic moment distribution formed in the grain boundary due to exchange interaction between neighboring grains with different easy axis orientations. The calculated full hysteresis coercivity  $H_{cm}$  ( $=0.14H_K$ ) is in reasonable agreement with available experimental data, where  $H_K$  is the anisotropy field. Both the calculated remanence  $M_r$  and coercivity  $H_c$  increase rapidly with the maximum applied field  $H_m$  at lower field ( $H_m < H_{cm}$ ) but exhibit gradual saturation at higher field. These results are consistent with the so-called nucleation type material. We demonstrate that this simple model, although neglects the long range magnetostatic interaction, can provide a realistic description of the magnetization and demagnetization processes in nanostructured permanent magnets by comparing our calculations with the experimental data for various forms of rapidly solidified Nd–Fe–B permanent magnets. The calculated  $M-H$ ,  $M_r-H_m$  and  $H_c-H_m$  curves show excellent agreement with the experimental data of hot pressed and die upset Nd–Fe–B magnets, where  $M_r$  and  $H_c$  are the remanence and coercivity, respectively.

© 2004 Elsevier B.V. All rights reserved.

**Keywords:** Hybrid model; Nanostructured permanent magnets; Magnetization and demagnetization

## 1. Introduction

Nanostructured permanent magnets aroused much interest in recent years because of their potential application such as recording media and micromechanical devices [1–3]. To understand

better the process of magnetization and demagnetization and the related coercivity mechanism is crucial to the efficient use of such material. The present understanding based mainly on the SW model (Stoner and Wohlfarth model), which treats the magnetic grains as non-interacting isolated grains and is sometimes over simplified and yields discrepancies [4–13]. The domain wall pinning (the presence of hindrances to domain wall displacement) and nucleation model (the nucleation of

\* Corresponding author.

E-mail address: maszgp@nus.edu.sg (G.P. Zhao).

reversely magnetized volume) are offered as alternatives [5–8]. These complicate micromagnetic models include the interactions and grain shape factor, which in many cases, cannot give the important underlying physics or analytical results. In view of this, we feel it necessary to make a compromise between the simplicity and accuracy.

In this paper we investigate the process of the magnetization and demagnetization based on a hybrid model. The reversible change of magnetization is governed by the SW model. A domain wall like magnetic moment distribution–transition region (TR) is formed at the interface between neighboring misaligned grains due to exchange interaction. Such TRs have been found in experiments [9,11] (where it is called multigrain domain wall). The TR moves reversibly between grain boundaries in the under-critical state. At a sufficiently large applied field  $H$ , the TR will propagate, initiating the nucleation of a domain wall near the grain boundary and drive the magnetic reversal of the whole grain through the motion of the domain wall. The role of misaligned grains played here is similar to the defects in nucleation model and can significantly increase the initial susceptibility and decrease the coercivity [12,13].

## 2. The calculation model

The model for the calculation has been addressed in detail in the previous papers [12,13] and explained the full hysteresis coercivity of nanostructured permanent magnets well. We give a brief description here. There are two basic assumptions of our model: (1) the reversible change of magnetization can be described by the SW model and (2) the TR can move between neighboring grains provided such motion is energetically favorable.

Two neighboring grains (grain 1 and grain 2) with uniaxial easy axis orientation  $\alpha_1$  and  $\alpha_2$ , where  $\alpha_1 < \alpha_2$ , are first considered. To resolve any directional ambiguity,  $\alpha_i$  will be taken as the effective easy axis orientation, i.e., the orientation that makes an acute angle with the magnetization orientation. Thus, by this definition, (magnetic)

reversal of a grain also reverses its effective easy axis directions. A grain will be said to have a positive easy axis if  $\alpha_i < 90^\circ$ , or negative otherwise. In the following all easy axis directions refer to the effective ones.

At a critical state, it can be shown that the TR will move and embed itself entirely within grain 1 if the following equation for grain 1 is satisfied [12,13]

$$E_1(\theta_2) = E_1(\theta_1) - [E_2(\theta_2) - E_1(\theta_2) + K \sin(\alpha_2 - \alpha_1)]. \quad (1)$$

The energy considered here include crystalline anisotropy energy and Zeeman energy,  $E_i(\theta_i) = K \sin^2(\theta_i - \alpha_i) - HM_S \cos \theta_i$ , where  $K$  is the crystalline anisotropy constant and  $M_S$  is the saturation magnetization. The first term of right side of Eq. (1) expresses the original energy of grain 1 while the left represents its energy in its new state in which the magnetization has rotated from  $\theta_1$  to  $\theta_2$ . The second term on the right-hand side of Eq. (2) reflects the effect of the energy barrier, in hindering the motion of the TR. The magnetization of the grain 1 will be reversed at this critical state, which begins with the motion of the TR, followed by the nucleation and subsequent propagation of a domain wall. The whole process is an irreversible magnetization change of grain 1 from one energy minimum state to the other.

The energy barrier, which hinders the motion of the TR, is much smaller than that corresponding to the coherent rotation [13]. For sufficiently small grains the energy barrier that hinder the motion of the TR will be overcome through the help of the thermal activation. And the critical field can be determined roughly by

$$E_1(\theta_2) = E_1(\theta_1). \quad (2)$$

The critical fields  $H_{\text{crit}}^{T=0}$  and  $H_{\text{crit}}^{\text{min}}$  determined from Eqs. (1) and (2), respectively, have been calculated for arbitrary easy axis combination (located in the same plane as the applied field). Fig. 1(a) shows the calculated reduced critical field as a function of  $\alpha_2$  with  $\alpha_1$  fixed at  $0^\circ$ . The critical field difference  $H_{\text{crit}}^{T=0} - H_{\text{crit}}^{\text{min}}$  is small and the maximum difference is only  $0.08H_K$ . This small critical field

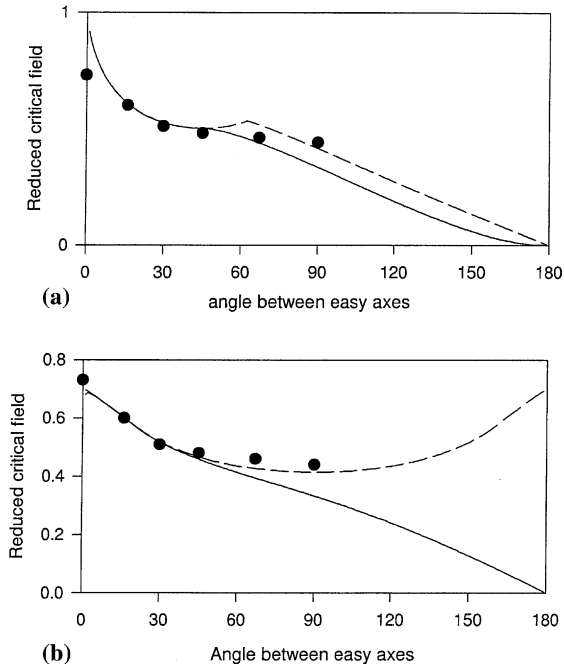


Fig. 1. The calculated critical field as a function of easy axis difference: (a)  $\alpha_1 = 0^\circ$ ; (b)  $\alpha_2 = 90^\circ$ . Numerical results (solid circle) of Ref. [8] are shown for comparison: (solid line)  $H_{\text{crit}}^{\text{min}}$  and (dashed line)  $H_{\text{crit}}^{T=0}$ .

difference leads to the similar behavior of smaller and larger grains in the initial magnetization process (Section 3).

In Fig. 1(b)  $\alpha_2$  is fixed at  $90^\circ$ .  $H_{\text{crit}}^{\text{min}}$  decreases continuously with easy axis difference. However,  $H_{\text{crit}}^{T=0}$  is an even function of  $\alpha_1$  and the minimum is  $0.414H_K$  at  $\alpha_1 = 0$  ( $\alpha_2 - \alpha_1 = 90^\circ$ ). Here the critical difference could be as large as 0.7. Such a big difference can explain grain size dependence of coercivity in nanoscale materials [13].

In the above calculation we considered two extreme cases: in the first case ( $H_{\text{crit}}^{\text{min}}$ ), the grains are small enough so that the energy barrier can be totally overcome by the thermal activation and the critical field for magnetization reversal obeys Eq. (2). In the second case ( $H_{\text{crit}}^{T=0}$ ), the grains are sufficiently large and the thermal effects can be ignored completely and the critical field obeys Eq. (1). In the real material, there is some distribution of grain size and the behavior of magnetization and demagnetization is in between. These two ex-

treme cases are also adopted for the calculation of a full hysteresis loop and the calculation procedure is arranged as follows. First we create a  $100 \times 100$  cubic grains with in-plane random easy axes and random magnetic orientations (either in the positive easy axis direction or in the negative easy axis direction) in the thermally demagnetized state. This corresponds to a thin film with random in plane easy axis distribution. The applied field increases gradually and the magnetic moment rotates according to the SW model until the critical field criterion, Eq. (1) (for big grains) or Eq. (2) (for small grains) is satisfied, when the grain reverses its magnetization and the corresponding easy axes change from negative to positive. Note that for every grain there are normally four neighboring grains and thus four critical fields, and the magnetization reversal takes place at the smallest of these four. This procedure is repeated until all negative easy axes change to positive and the whole system then approaches saturation according to the SW model. The calculation of the demagnetization curve is similar. When the field decreases gradually, the first quadrant demagnetization curves obeys the SW model (i.e., no grain reverses its magnetization). The magnetization reversal takes at the second and the 4th quadrant. A similar method has been used in the calculation of the magnetization and demagnetization of the partially magnetized material.

### 3. Initial magnetization and susceptibility

Fig. 2 shows the calculated initial magnetization curves. The solid line shows the initial magnetization behavior of small grains. The low-field susceptibility  $\chi = M/H$  is very large. Take the parameters of Nd-Fe-B as an example, the anisotropy constant  $K = 4.3 \times 10^6 \text{ J/m}^3$  and the saturation magnetization  $4\pi M_S = 1.61 \text{ T}$ . For  $H = 0.01H_K$  (671Oe),  $M = 0.15M_S$  and  $\chi = 28.7 \text{ (G/Oe)}$ . An increase of  $H$  leads to gradual decrease of  $\chi$ . For  $H = 0.1H_K$ , the magnetization  $M$  surpasses half of the saturation value and  $\chi = 9.93 \text{ (G/Oe)}$ . The larger initial susceptibility characterizes the properties of the so-called nucleation-type magnets, which is reasonable since in our model

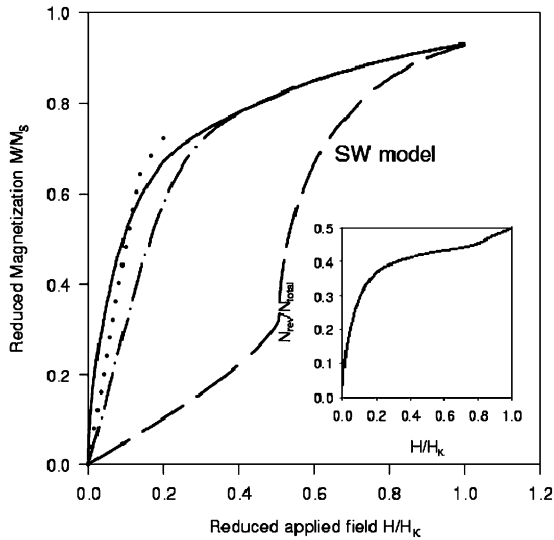


Fig. 2. Calculated initial magnetization curves: (solid line) small grains and (dashed line) large grains. The experimental data (dotted line) and the prediction of the SW model (dashed line) are shown for comparison. The inset shows the percentage of grains reversed as the function of the reduced applied field.

inhomogeneities within the grains are ignored and thus the motion of the domain walls (once nucleated) is completely easy. However, the approach to saturation magnetization is slow due to random alignment, which prevents the saturation at low fields. Thus such a magnetization has the attributes of both nucleation and pinning.

The large grains display similar initial magnetization behavior, which is given by the dash-dotted line. The low-field susceptibility is slightly smaller because the critical fields for large grains are slightly larger (cf., Fig. 1). This similarity contrasts sharply with the fact that the coercivity of large grains ( $0.42H_K$ ) is much larger than that of the small ones ( $0.14H_K$ ).

These results compare favorably with experiment data [2] (dotted line in Fig. 2) and are significantly better than the prediction of the SW model (dashed line in Fig. 2). The experimental initial magnetization curve, where the applied field  $H$  and the magnetization  $M$  have been normalized by the respective theoretical values of  $H_K = 67070$  Oe and  $M_S = 1281$  G, is based on a 80 nm thick Nd–Fe–B thin film produced by Parhofer et al.

For  $H > 0.1H_K$ , the experimental susceptibility tends to be larger than our predictions, in part because the easy axis distribution is not entirely random as has been assumed.

The inset of Fig. 2 shows the calculated percentage of grains reversed as the function of reduced applied field. In the virgin state half the grains possess the positive easy axes while the other half have negative easy axes. With the applied field increased some of the grains with negative easy axes reverse. As a result more grains possess easy axes than negative easy axes. When  $H/H_K = 0.6$ , 80% of grains with negative easy axes has reversed.

The calculated initial magnetization curves could also be used to explain the magnetization behavior (Fig. 3) in various forms of rapidly solidified permanent magnetic materials [9]. It can be seen that the initial magnetizations of both hot pressed magnets and die upset magnets are in reasonable agreement with our calculated results.

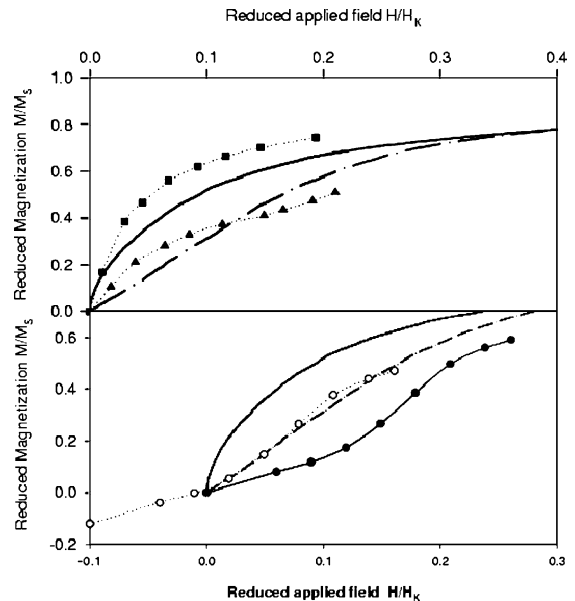


Fig. 3. (Top panel) Comparison of calculated initial magnetization curves for small (solid line) and large grains (dash-dotted line) with experimental data for hot-pressed (solid triangles) and die upset magnets (solid squares). (Bottom panel) Compares the theoretical data with experimental data for ribbons (solid circles). The shifted (see text for detail) data for ribbons (open circles) are in excellent agreement with theoretical data.

Both magnets possess a large initial relative susceptibility and decreases gradually with the applied field. The initial relative susceptibility of the die upset magnet is larger than the theoretical one while that of the hot pressed magnet tends to be slightly smaller than the theoretical value, which can be attributed to the different easy axis distributions. The degrees of alignment of the oriented die upset magnet and the isotropic hot pressed one was estimated as 85% [9] and 50%, respectively. Here our results are based on the plane isotropic case where the degree of alignment is estimated as 63.7% (the estimation is based on the maximum reduced remanence). The larger the degree of alignment, the more chances for neighboring grains to have larger easy axis difference and the smaller the average critical field, which leads to higher initial susceptibility.

The initial susceptibility of the ribbons, however, is much smaller compared with our theoretical results. Moreover, the initial relative susceptibility decreases with the applied field, which is in contrast with our theoretical curves. We believe that this low-field deviation of susceptibility is due to the pinning of the TR at small inclusions in the grain boundaries. This can be justified by the fact that if we shift the initial magnetization curve of ribbons to left by a distance of pinning field  $H_{\text{pin}}/H_K = 0.1$  [14], and downward by a distance equivalent to  $M/M_S = 0.12$  (which is roughly the experimental magnetization of ribbons at  $H = 0.1H_K$ ). The shifted curve agrees well with our calculated result.

#### 4. Field-dependent remanence and coercivity

The hysteresis loops for partially magnetized magnets have been calculated and compared with experiment. The details will be given elsewhere. Here, we give the calculated field dependent remanence and coercivity for small grains (Fig. 4), which highlight the demagnetization behavior of the material. As the maximum applied field  $H_m$  increases, both the remanence and coercivity increase and saturate gradually at about  $H_m = H_{\text{cm}}$ . These results are also in good agreement with the experimental data [9] of hot-pressed and die upset

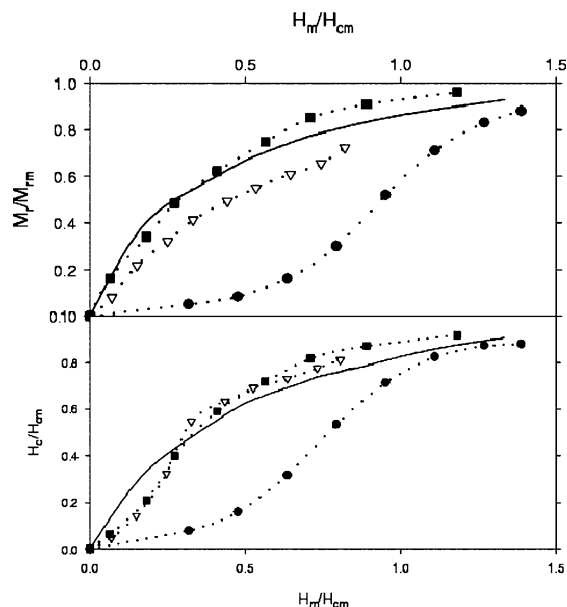


Fig. 4. Top: comparison between calculated field dependent remanence (solid line) and experimental data of ribbons (solid circles), hot-pressed (open triangles) and die upset magnet (solid squares). Bottom: comparison between the theoretical coercivity and experimental data.

Nd–Fe–B magnets. While the properties for the former are slightly inferior to the theoretical results, the latter tend to be better due to different texture. Both the low-field remanence and coercivity are much smaller for ribbons. Here again the shift of  $\Delta H = 0.1H_K$  is needed to obtain a good agreement. This feature is consistent with that in the initial magnetization curves and demonstrates that the governing mechanism for demagnetization is similar to that for magnetization, i.e., the motion of the TR.

#### 5. Conclusions

The magnetization and demagnetization process for Nanostructured permanent magnets can be well approximated through a hybrid model where the reversible change in the hysteresis loop is given by the SW model while the irreversible change is triggered through the motion of the TR. The nucleation of reversed magnets at the defects

and pinning of the TR in the grain boundary can affect the magnetization and demagnetization curves quantitatively. For example, while the coercivity of a material composed of large grains might be reduced considerably by the nucleation at defects, through the decrease of the critical field locally which change the mechanism of first reversal from that of our model, the subsequent propagation of such a reversal still obeys this hybrid model qualitatively. The initial magnetization and demagnetization curves are consistent with experimental data.

## References

- [1] S. Parhofer, C. Kuhrt, J. Wecker, G. Gieres, L. Schultz, J. Appl. Phys. 83 (1998) 2735.
- [2] S.M. Parhofer, J. Wecker, C. Kuhrt, G. Gieres, IEEE Trans. Magn. 32 (1996) 4437.
- [3] S.N. Piramanayagam, M. Matsumoto, A. Morisalo, S. Takei, J. Appl. Phys. 85 (1999) 5898.
- [4] E.C. Stoner, E.P. Wohlfarth, Philos. Trans. R. Soc. A240 (1948) 599.
- [5] H.J. Buschow, in: E.P. Wohlfarth, K.H.J. Buschow (Eds.), Ferromagnetic Materials, vol. 4, Elsevier Science Publications, Amsterdam, 1988, pp. 1–130.
- [6] D. Givord, M.F. Rossignol, in: J.M.D. Coey (Ed.), Rare-earth Iron Permanent Magnets, Oxford Science Publications, 1996, pp. 218–285.
- [7] A. Aharoni, Introduction to the theory of ferromagnetism, Oxford University Press, 1996, pp. 183–214.
- [8] T. Schrefl, H.F. Schmidts, J. Fidler, H.K. Kronmüller, J. Magn. Magn. Mater. 124 (1993) 251.
- [9] P.E. Pinkerton, D.J. Van Wingerden, J. Appl. Phys. 60 (1986) 3685.
- [10] A. Manaf, R.A. Buckley, H.A. Davies, M. Leonowicz, J. Magn. Magn. Mater. 101 (1991) 360.
- [11] G.C. Hadjipanayis, W. Gong, J. Appl. Phys. 64 (1988) 5559.
- [12] C.K. Ong, Y.P. Feng, G.P. Zhao, H.S. Lim, D. Wei, J. Appl. Phys. 87 (2000) 5532.
- [13] G.P. Zhao, H.S. Lim, C.K. Ong, Y.P. Feng, G.R. Liu, J. Appl. Phys. 91 (2002) 2186.
- [14] H. Zijlstra, in: E.P. Wohlfarth, K.H.J. Buschow (Eds.), Ferromagnetic materials, vol. 3, Elsevier Science Publications, Amsterdam, 1988, p. 79.